RESEARCH ARTICLE

Effectiveness of Neural Fault Detectors of Permanent Magnet Synchronous Motor Trained With Symptoms From Field-Circuit Modeling

MACIEJ SKOWRON[ID]**, MATEUSZ KRZYSZTOFIAK**[ID]**, AND
TERESA ORLOWSKA-KOWALSKA**[ID]**, (Life Senior Member, IEEE)**
Department of Electrical Machines, Drives and Measurements, Wroclaw University of Science and Technology, 50-370 Wroclaw, Poland

Corresponding author: Maciej Skowron (maciej.skowron@pwr.edu.pl)

ABSTRACT Permanent magnet synchronous motors (PMSMs) are increasingly used in industrial drive applications. However, these motors can also undergo various failures, causing production line downtime and resulting in economic loss. Modern diagnostic systems allow the analysis of technical conditions based on a dataset containing fault symptoms. In most cases, the development of diagnostic patterns indicates the necessity for interference in motor mechanical construction. This fact speaks to the use of mathematical models, particularly those based on finite-element methods. This study investigated the possibility of fault classification using self-organizing Kohonen maps and a multilayer perceptron, based on training with data from a field-circuit model. The objective of this study is to demonstrate that such neural systems can detect and classify real motor faults under different operating conditions. Research has focused on stator-winding faults, demagnetization, and mixed faults. Experimental tests demonstrated the impressive diagnostic capability of the shallow neural networks developed for diagnostic tasks.

INDEX TERMS Demagnetization, faults diagnosis, finite element method, interturn short-circuits, multi-layer perceptron, permanent magnet machines, self-organizing feature maps, spectral analysis.

I. INTRODUCTION

Currently, one of the main factors determining the productivity of industrial drive systems is their reliability, and it is possible to continuously monitor the state of machines in real time. Currently, industrial drive management systems must ensure a high production efficiency, rapid response to failures, and easy and effective operation of the entire production line. Combined with the idea of Industry 4.0, in which we register a number of parameters related to the technological sequence, this leads to an increasing emphasis on diagnostic applications for electric drive systems.

Induction motors and permanent magnet synchronous motors (PMSM) are becoming increasingly popular machines used in industrial drive systems, as well as in commercial applications [1]. Despite the many similarities

The associate editor coordinating the review of this manuscript and approving it for publication was Gerard-Andre Capolino.

between electrical circuits and mechanical constructions, it is not possible to use diagnostic patterns (symptoms) directly from one machine to another. Currently, the development of modern diagnostic applications includes the use of artificial intelligence techniques based on information regarding the diagnostic patterns. Only correctly selected diagnostic symptoms allowed for correct assessment of the technical conditions of the machine. However, the extraction of universal fault symptoms that can be implemented in diagnostic applications of different AC motors remains an unrecognized field of study.

The search for individual symptoms of electric motor damage is mostly connected to two methods: physical modeling of the fault on the real object and mathematical modeling of the machine with the included defect. However, the physical modeling of machine failures through the degradation of individual components is relatively simple in practical execution; it does not allow one to understand the exact mechanisms of

defect formation. The physical failure of a machine to create a comparison pattern also involves generating costs as well as the resulting pattern degradation with subsequent testing of the machine. To eliminate these limitations, mathematical models of electric machines are typically used [2]. They provided key information regarding the phenomena that occur in the tested object without interfering with the electromechanical system. This solution also applies to approaches used in the diagnosis of PMSM drives [3].

The mathematical models of PMSM discussed in the literature can be divided into two main groups: circuit models that include the equivalent circuit analysis of the motor [4], [5], [6], [7], [8] and models based on computationally more complicated finite element methods (FEM) [9], [10], [11]. This classification shows two directions for modeling phenomena that occur in electrical machines. The first approach is based on the electrical equivalent circuit of the motor windings, considering the constant lumped parameters consistent with the simplifying assumptions used. However, because of the simplifications made at the stage of formulating this model, it does not reflect all the phenomena occurring in the machine, particularly the electromagnetic phenomena. As a result, the circuit model does not require long computation time and is perfect for testing drive systems for which a large number of simulations are performed.

The second approach is based on algorithms for determining the electromagnetic field distribution in the machine, which makes it possible to calculate the sources of electromotive forces, considering the nonlinear phenomena occurring in the magnetic circuit. The FEM is currently the most advanced technique for modeling electrical machines that require high computing power. The combination of the precision of the FEM model to solve magnetic field equations and the simplicity of the concept of a circuit model have been used in field-circuit modeling methods [12], [13].

In diagnostic applications, FEM models are used only as reference points for methods that are based on the measured signal of the tested object. These techniques are based on the residual between the model and response of an object that is not resistant to enhanced amplitudes of noise, imperfections in mathematical modeling, and small changes in the parameters of the object during operation.

Owing to the differences in the values of damage symptoms between the FEM model and real objects, which result in difficulties in assessing motor technical conditions, neural networks can be used. To the best of our knowledge, solutions using FEM models for PMSM fault pattern acquisition are rare.

Furthermore, examples of the implementation of FEM-based fault symptoms as a neural network (NN) training data packet and validation of a real object presented thus far in the literature do not provide satisfactory results. As presented in [14], fault features extracted by analytical methods such as spectral analysis cannot be used for fault diagnosis, particularly in the case of incorrectly modeled motor geometry.

This fact is related to the task that the NN must perform: the data approximator [15], [16] or the classification system [13], [17], [18], [19], which is related to the proper choice of the neural structure. However, the selection of the type of NN structure also depends on many factors related to the practical implementation of the diagnostic application, such as the diagnostic function, computing capacity, and motor operating conditions [15]. These parameters have a significant influence on the precision of the decision-making processes and the dynamics of the training process. Furthermore, the dynamics of the network training process are closely related to the appropriate selection of training data.

In the practical implementation of an NN-based fault detection system, methods based on the application of training data from a mathematical model for both training and validation are often used [20], [21]. However, such an approach is characterized by a very high training accuracy and high dynamics of the training process but relatively low effectiveness when testing the network on a real object. This phenomenon is observed especially in the case of significant differences in data between models and real measurements, for example, owing to measurement noise or imperfections in the model. A common technique is to use data derived from measurements of a real object in both teaching and testing NN [14], [15], [16], [19], [22], [23], [24], [25], [26], [27]. Therefore, during the training process, the NN acquires the ability to generalize, which gives the precision of the network for the analyzed object a very high value. The disadvantage of this method is the need to complete the process in the case of an analysis of a new type of damage. In addition, this method causes physical damage to a real object to obtain new diagnostic patterns. It should be emphasized that the idea of physical modeling of damage, unlike the use of mathematical models, does not allow one to recognize the initial stages of damage.

Based on the limitations mentioned in the PMSM diagnostic system based on the FEM model and shallow NN [14], this study demonstrates the possibility of using FEM combined with circuit modeling of the PMSM with stator winding and permanent magnet (PM) faults for the preparation of fault signature datasets. Damage symptoms constitute elements of the input vectors of the self-organizing Kohonen maps and the multilayer perceptron classifier. It should be emphasized that the field-circuit model of the PMSM was used only for the preparation of training vectors for the analyzed NNs. Testing of the developed neural fault detectors and classifiers was carried out by experimental verification of a real drive system. During the studies, three types of PMSM motor damage were analyzed: interturn short- circuits (ITSC), demagnetization, and mixed defects. Experimental verification of the proposed NN-based diagnostic applications was carried out on a specially designed laboratory stand with a 2.5 kW PMSM.

This study is divided into five sections. In the second section, an analysis of the PMSM mathematical model and its experimental verification are presented. The analysis of the FEM-circuit model and the concept of modeling the stator

and rotor faults are described. Furthermore, an experimental verification based on the motoring and generation modes of the developed model was presented. The high precision of the PMSM modeling was confirmed by comparison with measurements performed on a real object. The third Section describes the extraction of fault symptoms based on the fast Fourier transform of the stator current signal obtained from the field-circuit modeling of the PMSM drive and experimental tests. The experimental tests are presented for comparison. The spectrum analysis was performed under different PMSM operating conditions. The amplitudes of the stator current spectrum obtained from FEM-circuit modeling constitute the elements of the NN input vectors, as described in the next section. The concept of a fault classification system based on self-organizing Kohonen maps and a multilayer perceptron is discussed in two separate parts of the fourth section. In this section, which constitutes the main part of this article, the training process of two different types of shallow NN based on information from PMSM modeling and subsequent tests on the real object are presented. The precision of the NN-based PMSM diagnostic system can be classified into two categories: fault detection and damage classification. The article is completed with a summary of the experimental results of the proposed diagnostic application based on an FEM-circuit model supported by shallow neural networks.

II. PMSM FAULT MODELING BASED ON THE FEM AND CIRCUIT-BASED SIMULATION

A. DESCRIPTION OF THE PMSM MODEL

Currently, motor modeling is based on the use of the FEM approach, which allows high-precision representation of the phenomena that occur in real machines. The PMSM model was constructed using the ANSYS Maxwell environment. The geometry of the tested device was split into disjoint and non-overlapping components of a simple geometry called finite elements, where electromagnetic circuit calculations were performed at each grid point. Calculations based on the analysis of the FEM model make it possible to determine the distribution of the magnetic field in the individual parts of the machine. The data generated consider the properties of the materials used to build the machine, and the consideration of multiple factors makes it possible for this approach to provides an accurate and complete description of the electric motor. Simulations were performed in co-simulation mode with a field-oriented control (FOC) structure taken into account. The concept of coupling variables between FEM and circuit models is presented in Fig. 1.

The entire simulation was executed with a calculation step of 1e-4 s, and the controller parameters were set to the same value as that of the Lenze voltage inverters used in the research. The sampling frequency of the FEM-circuit model was 8192 (2^{13}) Hz, which made it possible to compare the simulation results with the results obtained on a real object and the preparation of training and testing data for the analyzed neural networks.
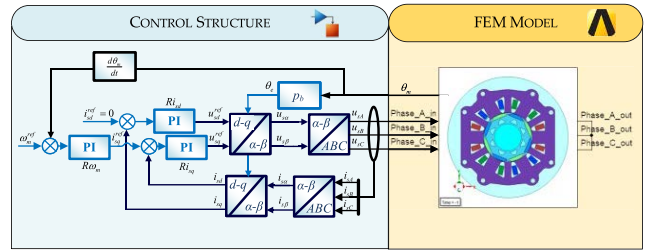

FIGURE 1. Schematic co-simulation diagram of PMSM drive with field-circuit model considering stator winding and rotor demagnetization faults in FOC structure.
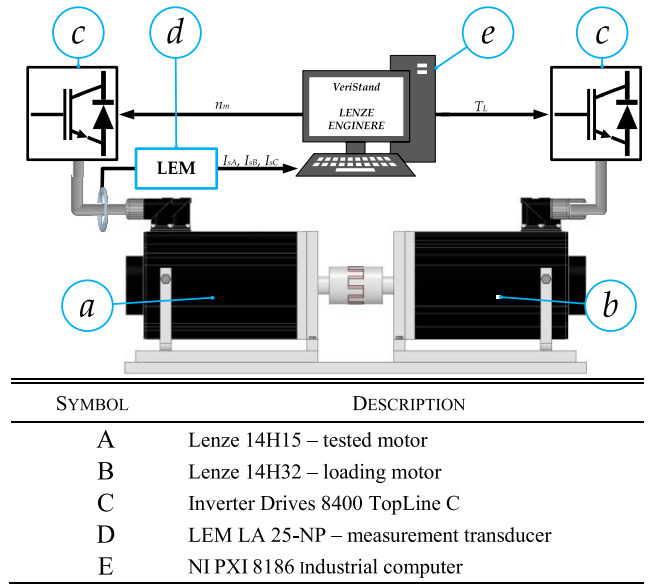

SYMBOL	DESCRIPTION
A	Lenze 14H15 – tested motor
B	Lenze 14H32 – loading motor
C	Inverter Drives 8400 TopLine C
D	LEM LA 25-NP – measurement transducer
E	NI PXI 8186 industrial computer

FIGURE 2. Experimental setup: schematic diagram of connections.

B. EXPERIMENTAL VERIFICATION OF THE PMSM SIMULATION MODEL

The simulation model was developed for a real 2.5 kW PMSM by Lenze with the specifications listed in Table 1. A schematic of the experimental test stand is shown in Fig. 2. The tested and loaded motors were powered by Lenze industrial voltage inverters operating in closed loops. The measurement data acquisition system was implemented using a DAQ NI PXI–4472 measurement card installed on an NI PXI 8186 industrial computer.

Motor failure analysis was performed using a specially designed test stand with a PMSM. Physical models of the stator and rotor faults are shown in Fig. 3. The modified PMSM design allowed physical modeling of ITSCs in phase B of the stator winding in the range of one to three shorted turns. The motor shown in Fig. 3a was used in the experimental tests. The leads of the individual coils of the PMSM stator winding and an example of ITSC fault realization in the form of three short turns are shown in Fig. 3b. Moreover, it was possible to change the rotor of the PMSM to model the partial demagnetization and mixed damage. Rotor failure is realized by removing a magnet fragment from a pair of permanent
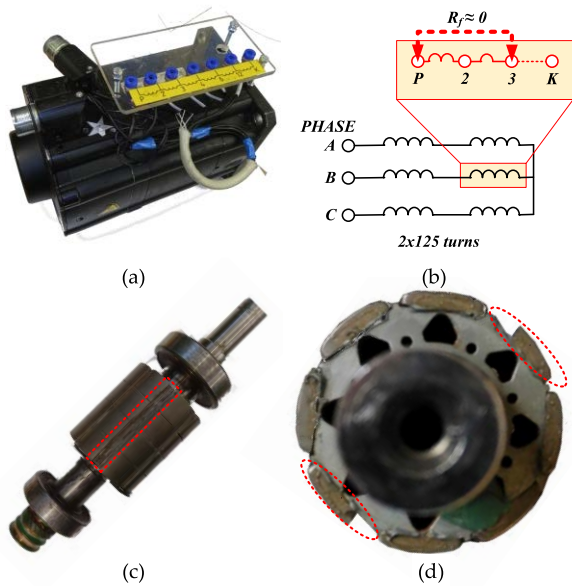
FIGURE 3. Experimental setup and real failure models for the investigated faults: (a), (b) PMSM with a special stator winding connector to model ITSCs; (c), (d) rotor with partial demagnetization.

FIGURE 4. Static characteristics of PMSM obtained with experimental tests and simulation model for f_s = 100 Hz: (a) phase current versus load torque and (b) phase-to-phase voltage versus load torque.

magnets. The side and front views of the rotor with the parts of the removed magnet are presented in Figs. 3c and d.

The results of the mathematical modeling were compared with the experimental results to prove the correctness of the developed field-circuit model of the PMSM. NN-based fault detectors and classifiers trained using simulation data were also tested on the measurement data obtained from the experimental setup.

The parameters and mapped geometry of the stator and rotor of the analyzed PMSM were used to build the FEM model. The data obtained from the simulation model were compared with those obtained from measurements in a real drive system. A comparison of the static characteristics of the phase currents and phase-to-phase voltages versus the load torque (T_L) from the FEM-circuit model and measurements of the experimental motor is illustrated in Fig. 4. The presented results show the difference in the respective signals during the change in load torque in the range of 0 to 120% T_{LN}. The relative error between the model and the real object was estimated to be in the range of 1% to 6% for phase currents, whereas for phase-to-phase voltages, the error was in the range of 2% to 8%. Thus, it was assumed that the developed PMSM model was sufficiently accurate to reflect the physical phenomena of the real motor. The basic model demonstrated here was modified to allow the modeling of the analyzed PMSM faults.

C. MODELING OF THE INTERTURN SHORT-CIRCUIT IN STATOR WINDINGS

The proposed PMSM model includes stator-winding failures. In Fig. 5, the *B* phase of the stator winding, where motor failures occur, is brightened. The fault was realized in phase B on
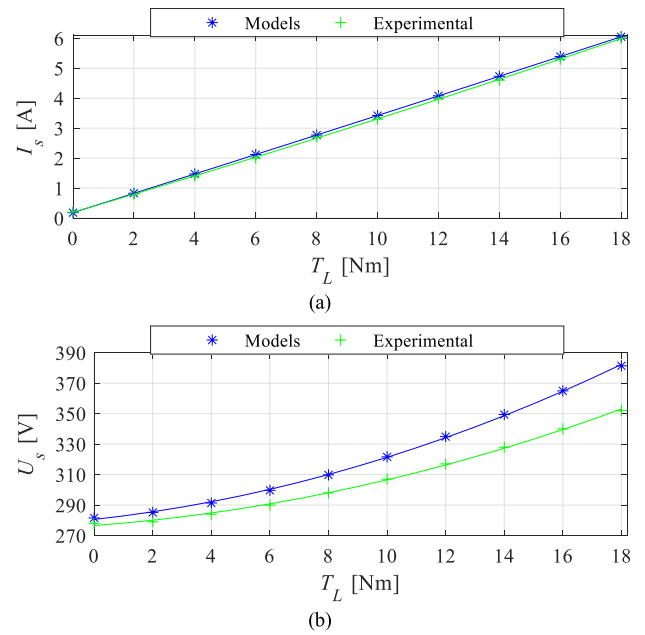
specially prepared leads from the stator coils. The simulation faults correspond to the analysis of the damaged object (with an incipient fault, N_{sh}, of 1–3 shorted turns).
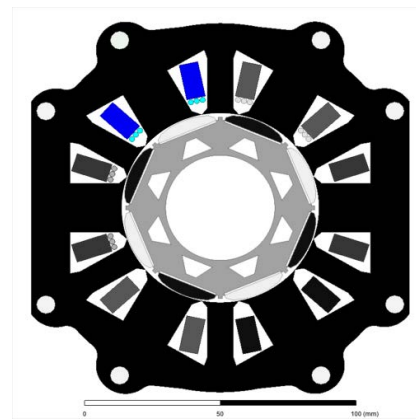

FIGURE 5. Cross-section of the analyzed motor, including the stator winding fault, FEM model allowing damage to N_{sh} = 1, 2, and 3 in the test phase.

An example of a short circuit model is shown in Fig.6. The tested motor circuit model can be divided into a mechanical part (blue box) and electrical part (green box). A section of the coils (N_{sh} = 1,2,3) was extracted from the stator winding in Phase B, through which the coil short circuits were modeled. In the undamaged state, only the operating current I_s flows through the motor windings, whereas an additional fault circuit is created in the faulty state. The Modeling of the stator winding damage was implemented with an additional resistance R_f, changing the value from 10 MΩ to 1 mΩ. The R_f values correspond to the insulation resistance values
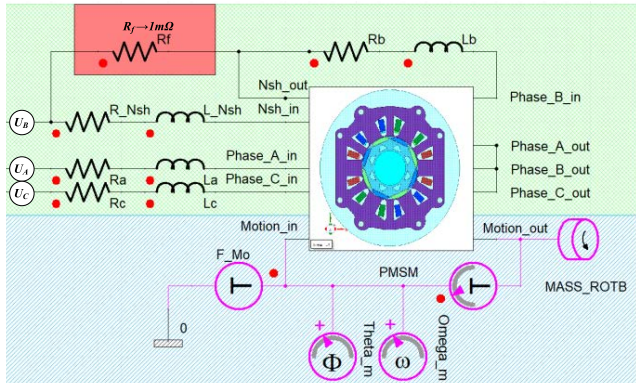
FIGURE 6. Model of PMSM in ANSYS Electronics with marked mechanical parts (blue box) and electrical parts (green box).

for an undamaged winding and ITSC fault, respectively. The modeling method presented here is similar to that used in other research centers [28].
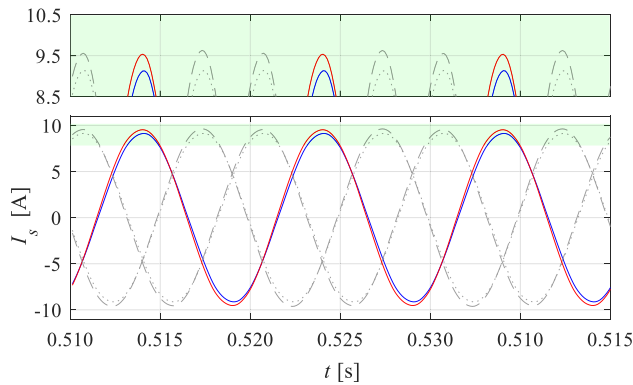

FIGURE 7. Instantaneous values of the stator phase-current waveforms in the case of a healthy winding and with three short-circuited turns of phase B: $f_S = 100$ Hz, $T_L = T_{LN}$: blue line - unfaulty state, red line - faulty state.

The ITSC fault results in asymmetry in the stator winding of the PMSM. This asymmetry was observed in the phase currents, as shown in Fig. 7. A comparison of the undamaged motor case and the motor with three shorted turns clearly showed an increase in the current amplitude (approximately 4%).

D. MODELING OF THE PM DEMAGNETIZATION

A PMSM rotor is typically demagnetized because it exceeds the allowable operating temperature of the machine associated with the applied PMs (Curie temperature). This phenomenon is observed during high-overload motor operations as well as during ITSC. Additionally, damage to magnets can occur when they fail as a result of mechanical impact.

Regardless of the type of failure in the magnets, the strength of the electromagnetic field decreased at the moment of the fault. The failure case of one pair of PMs mounted on the rotor of the tested PMSM is illustrated in Fig. 8. The percentage of damage to the magnets corresponds to the color scale presented in Fig. 8, and the percentage value
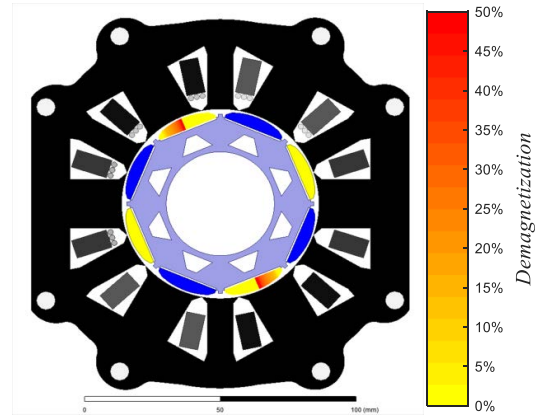

FIGURE 8. Cross-section of analyzed motor considering demagnetization fault. The percentage of the PM area removed is indicated by the color legend.

corresponds to the volume reduction related to one magnet. The effect of demagnetization is clearly visible in the back electromotive force (BEMF) generated when the PMSM operates in generating mode. A comparison of the simulation and experimental results for the PM fault in the tested PMSM is shown in Figure 9. The generated electromotive force corresponded to the removal of approximately 25% of the PM area from one pair of magnets.
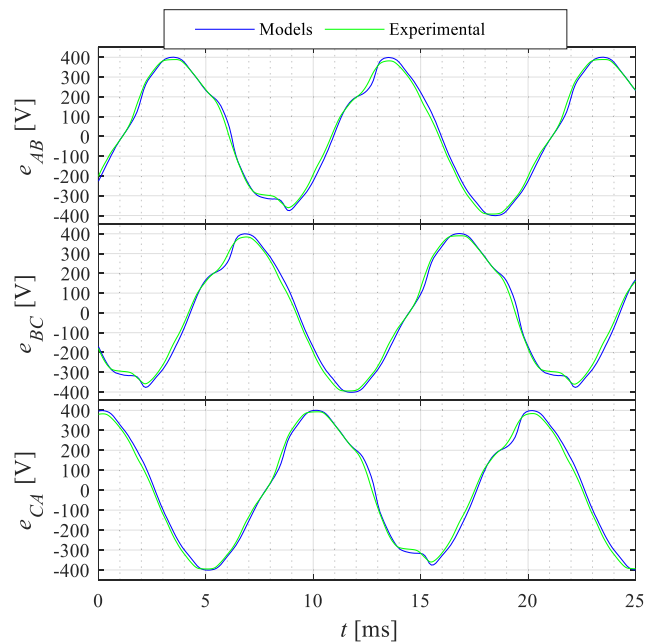

FIGURE 9. Electromotive force generated by the PMSM for permanent magnet damage during simulation and under experimental conditions for n_{ref} = 1500 rpm.

The simulated waveforms of BEMF are shown in Fig. 10. Failures to PMs in the range of 0–50% are visible on the waveforms of the generated voltages. Typical deformations caused by the failure of the PMs, periodically repeated in each phase of the generated voltage, are marked and magnified in Fig. 10b.
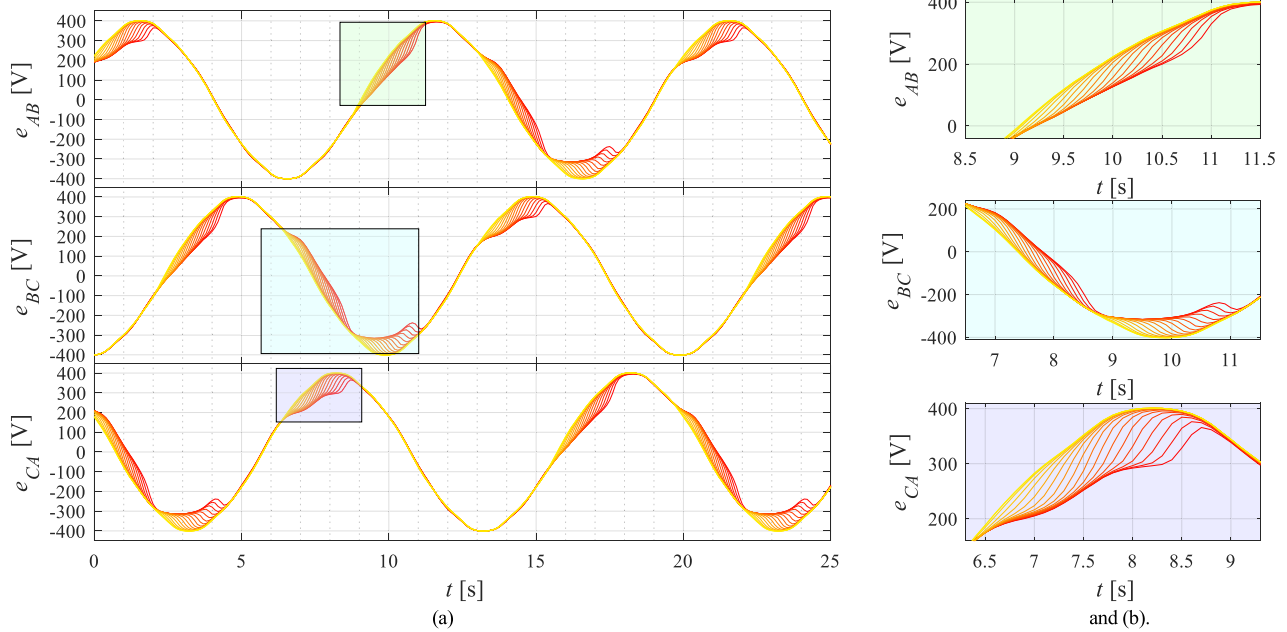
FIGURE 10. BEMF waveforms for the motor with a demagnetization fault calculated under simulation conditions depending on the percentage of PM damage: (a) BEMF transients for n_{ref} = 1500 rpm and (b) zooms.
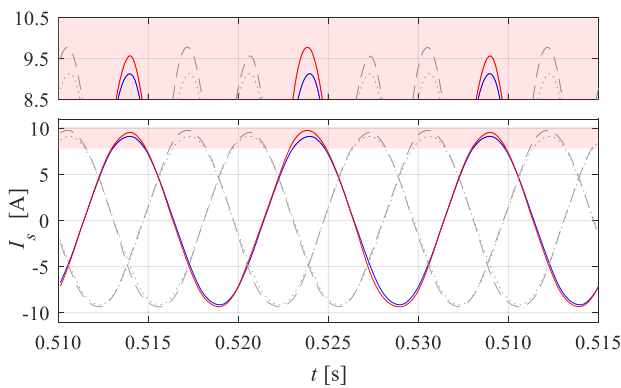

FIGURE 11. Simulated transients of the stator phase current in the case of partial 6% demagnetization: f_s = 100 Hz, $T_L = T_{LN}$: blue line, unfaulty state; red line, faulty state.

FIGURE 12. The cross-section of the motor was analyzed considering the simultaneous fault of the PMSM stator windings and PM demagnetization; N_{sh} = 1, 2, 3, and demagnetization at a level of 6%.

The characteristic deformations of the electromotive force observed in the simulation correspond to the experimental results. Based on these results, it can be concluded that the developed field-circuit model correctly reproduced the phenomena observed in a real motor. A comparison of the simulated stator current signals for an undamaged and a partially demagnetized motor is shown in Fig. 11.

E. SIMULTANEOUS FAULTS TO STATOR WINDING AND PM

Another analyzed fault state was the simultaneous damage to the stator winding and the magnets of the PMSM drive. The occurrence of mixed faults leads to the appearance of fault symptoms visible in the motor current, which are specific to demagnetization and ITSC. In Fig. 12, a cross section of the motor in the FEM model considering the simultaneous failures of the stator and rotor is presented. The analysis of
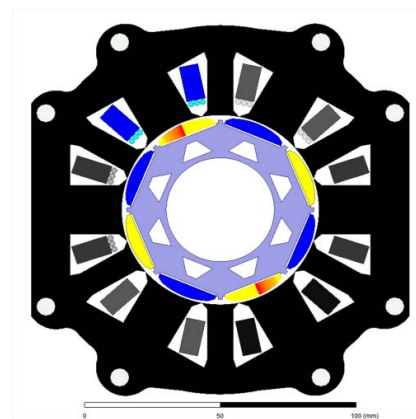
mixed-fault operation is important because the development of winding short circuits causes local temperature changes, which, combined with operation under full-load conditions, leads to a widening of the demagnetization. On the other hand, the development of the demagnetization level causes a change in the generated BEMF and causes the motor to operate with the same load torque as in the case of the undamaged motor. It is necessary to force a larger phase current, which leads to an increase in the temperature of the entire motor winding.

In Fig. 13, the waveforms of the phase currents for a PMSM with mixed faults are presented. The superposition of many faults is unfavorable and can cause problems in the interpretation and diagnosis of failures. The appearance of an ITSC and demagnetization cause an increase in
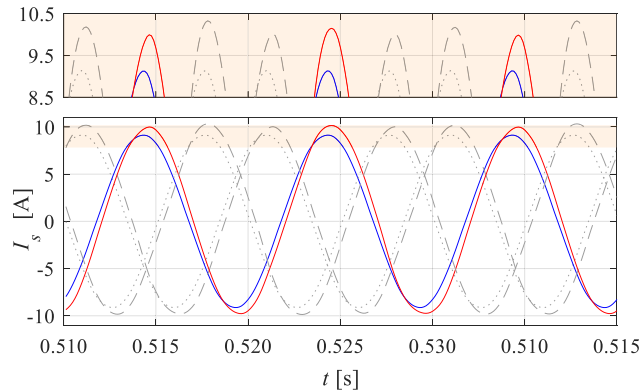
FIGURE 13. Waveforms of the stator phase current in the case of simultaneous partial demagnetization and short circuits of three turns in phase B; f_S = 100 Hz, $T_L = T_{LN}$; blue line: unfaulty state; red line: faulty state.

the instantaneous values of the stator current amplitudes, particularly in the faulty phase, and its distortion, analogous to the BEMF waveforms. This asymmetry indicates the appearance of additional harmonics in the phase currents.

III. EXTRACTION OF PMSM DAMAGE SYMPTOMS BASED ON THE FEM-CIRCUIT MODEL

The basic idea of electrical machine diagnostic systems is related to the continuous observation of changes in measured signals and evaluation of the trends of these changes. This approach requires a deep understanding of the impact of faults on diagnostic signals and extraction of fault indicators. Among all the known damage symptom extraction techniques, the fast Fourier transform (FFT) is still the most widely used [29]. This is due to the fact that FFT is a compromise between the precision of failure symptom assessment and computational complexity. In further parts of this research, FFT analysis will be used to extract failure symptoms from simulated current waveforms, which are elements of the SOM and MLP input vectors.

To demonstrate that the symptoms obtained from the field-circuit modeling of the analyzed damage can be used to develop neural fault detectors, they were compared with the symptoms obtained from the measurements of a real motor with the same damage performed on a laboratory stand described in the previous section.

Spectral analysis of the stator current enables the assessment of the technical condition of PMSM stator windings based on information regarding the amplitude values of the characteristic spectrum components (harmonics and subharmonics of the measured signal).

The degree of damage to the ITSC affects the amplitude at frequencies that are odd multiples of the fundamental frequency of supply voltage. In addition, changes in spectral amplitudes were observed at the frequencies described by the following equation:

$$f_{sh} = f_s \left(\frac{2k+1}{p_b} \pm m \right), \tag{1}$$

where:
f_s— fundamental frequency of the supply voltage,
p_b – number of pairs of poles,
$k = 1, 2, 3, \ldots,$
$m = 1, 3, 5, \ldots, 2p_b$-1.

The demagnetization fault causes harmonics related to the rotational frequency to appear, which in the PMSM motor is the multiplicity of the supply frequency.

$$f_d = f_s \left(1 \pm \frac{k}{p_b} \right) = f_s \pm k f_r, \tag{2}$$

where:
f_r – rotational frequency,
$k = 1, 2, 3, \ldots.$

The content of additional harmonics and sub-harmonics was determined by comparing the spectra of the phase currents for the state of damage (red line) and its absence (blue line). The analysis was performed for both the field-circuit model, which is the signal pattern source for NN training, and based on the measurements of a real object, which will be used further for testing the developed neural fault detectors and classifiers.

A comparison of the results of the spectral analysis presented in Fig. 14 directly shows the features of the considered PMSM defects. The analysis of Fig. 14a shows that the symptoms of stator damage are related to the third harmonic of the fundamental frequency (1) for both the signals coming from the model and those measured on the real object. Furthermore, the occurrence of the three ITSCs caused an increase in the amplitude of the mentioned component of the current spectrum by approximately 30 dB. In the spectrum of the measured signals shown in Fig. 14b, the effect of the three ITSCs resulted in an increase in the amplitude of the third harmonic of the fundamental frequency of approximately 6 dB.

The next step in the FFT analysis was to determine the characteristics of the signal related to the demagnetization. According to Equation (2), the symptoms of PM failure are primarily related to the rotational frequency and its multiples, as shown in Figs. 14b and 14c. The occurrence of demagnetization causes an increase in the amplitude of the phase-current spectrum components. Therefore, it should be noted that demagnetization does not significantly affect the amplitude of the third harmonic of the supply voltage, which is a symptom of stator-winding faults.

Analysis of the spectrum during mixed damage (Fig. 14e,f) confirms the possibility of selecting fault symptoms that are partially independent of each other.

However, the clear influence of damage to the PM on the spectrum of the phase currents makes it difficult to assess the technical conditions of stator windings. This was because of the small quantitative changes in the currents caused by the ITSC, especially in the initial stage. Therefore, the diagnosis of PMSM damage based only on FFT analysis is difficult, particularly during the operation of the drive system under variable loads and for different rotational speeds.
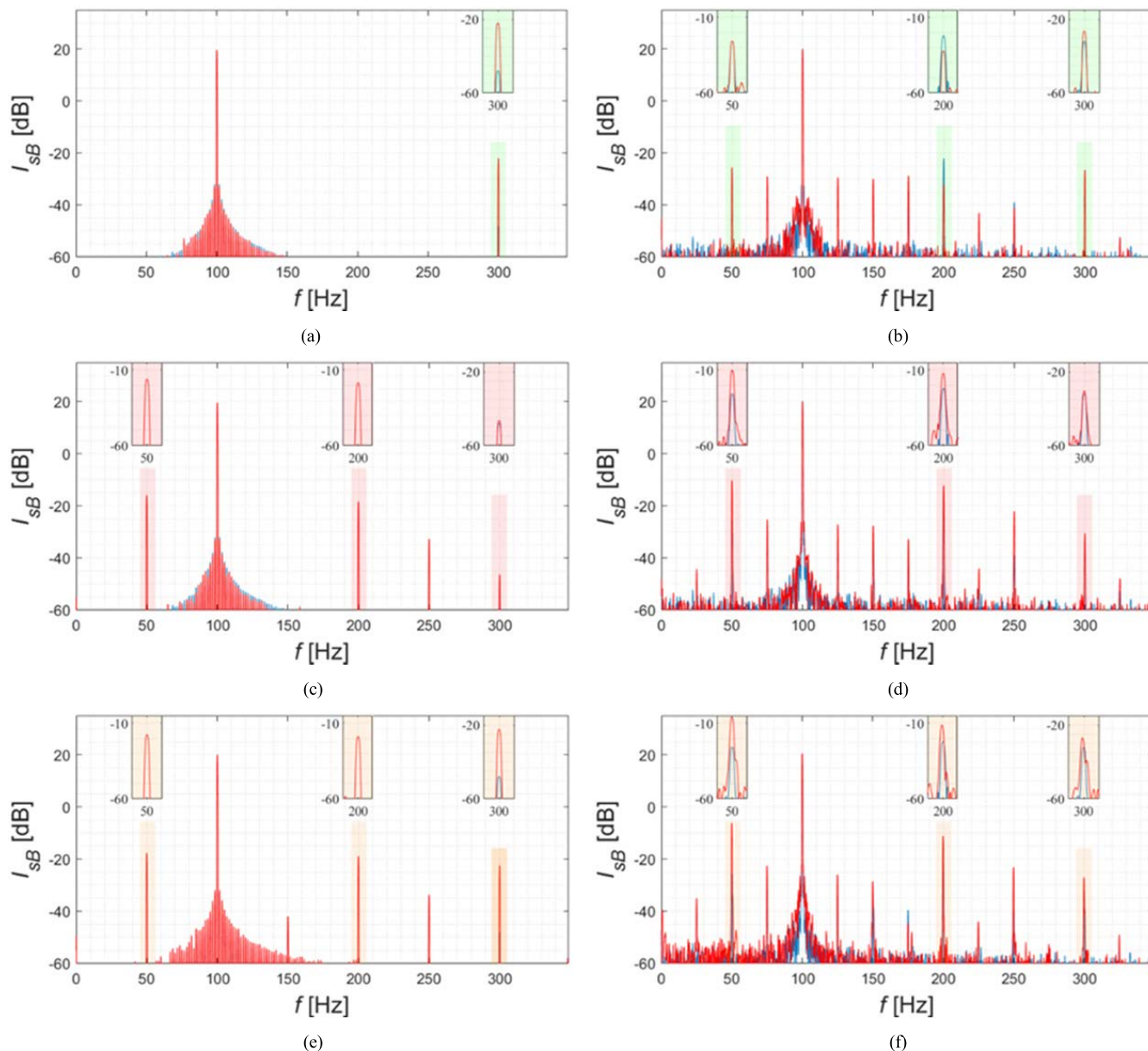
FIGURE 14. Spectral analysis of stator phase current obtained from FEM-circuit model (a, c, e) and a real PMSM drive (b, d, f): stator winding fault (a, b), 6% partial demagnetization (c, d), mixed faults (e, f); $f_s = 100$ Hz, $T_L = T_{LN}$: blue line-unfaulty state and red line-faulty state.

To partially automate the decision-making process, specific damage symptoms were further analyzed using NN-based detectors and classifiers.

The neural detectors developed in this study were constructed using *MATLAB* software, where data normalization, neural calculations, and an inference stage were performed.

IV. PMSM FAULT CLASSIFIERS BASED ON SHALLOW NEURAL NETWORKS

The use of classic neural structures, the training process of which is based on the results of mathematical modeling while verification takes place on a real PMSM, is rarely described in the literature [30], [31], [32]. This results from the difficulties in the development of NN input vectors that

are resistant to motor operating conditions and measurement noise. In most cases, these systems include only PMSM damage detection [31], [32] without fault classification. Furthermore, the analyses presented in the literature mainly cover cases of very serious failures that, in practice, result in the shutdown of PMSM [30], for example, phase failure [31] or phase-to-phase short circuits [32]. The stator winding damage presented in [30] results in an almost 50% increase in the phase current, which, from a practical standpoint, is useless owing to the earlier tripping of the motor overcurrent fuse. The following examples of the use of SOM and MLP in diagnostic systems, presented in this article, focus on both the detection of damage and the classification of its type. Furthermore, owing to the experimental verification of the

systems presented in the literature, based on a small number of examples [30], [31], [32], it was decided to show the operation of the developed NN-based systems for many more cases when the PMSM operating conditions changed.

Based on the author's experience with the application of shallow NN in the diagnosis of different AC motor winding faults [15], [16], [33], [34], we decided to use shallow neural structures in the form of SOM and MLP. In this study, particular attention was paid to the possibility of fault classification using the aforementioned NN structures, based on training with data from the field-circuit model.

A. THE IDEA OF FAULT CLASSIFIER BASED ON SELF-ORGANIZING KOHONEN MAPS

The primary function of SOM in diagnostic applications is to distinguish subsets of data with the same properties in a heterogeneous set of units. Determining clusters of units with similar characteristics allows for clear separation of subsets of the entire dataset.

The SOM consists of two layers: the input layer, which is composed of a vector of input data, and the output layer, which comprises neurons distributed in the network nodes.

During the studies, a map structure with dimensions of 20×20 and a rectangular topology was used. The SOM input vector contained normalized amplitudes in the range of $0-1$ of the current spectrum components with frequencies f_s, $3f_s$, $f_s + 2f_r$, $f_s + 10f_r$. The training process was performed based on 288 training samples covering four categories necessary for detection: unfaulty state, stator winding damage (initial ITSC: 1–3 shorted turns), demagnetization, and mixed damage (simultaneous fault of the permanent magnet and 1–3 shorted turns). Furthermore, the training vector contained samples for different values of the load torque ($T_L = (0-1)T_{LN}$ with $0.2T_{LN}$ step) and the frequency of the supply voltage (rotational speed ($\omega_m = (0.5-1) \omega_{mN}$ with $0.1\omega_{mN}$ steps)). The parameters of the SOM structure and training process are listed in Table 1.

TABLE 1. Parameters of self-organizing Kohonen maps.

Name of parameter	Value
Structure (number of neurons in axis X and Y)	20×20
Input vector size	1×4
Input vector normalization	[0,1]
Topology	Hexagonal
Training algorithm	WTM
Number of training epochs	1000
Initial neighbourhood radius	10
Neighbourhood function	Gaussian
Initial learning coefficient	0.7
Training data (simulation) packet size	288
Testing data (real measurements) packet size	288
Number of considered fault categories	8

The SOM training process was conducted for 1000 learning epochs and began by assigning random initial values to the weighting factors. The radius of the neighborhood used during the learning process was gradually reduced from an

initial value of 20. The process of adapting the weights of the neurons according to the winner takes the most (WTM) learning method as follows:

$$w_m(k + 1) = w_m(k) + \eta(k)G(R, d(c, m))[x(k) - w_m(k)],$$

$$(3)$$

where:

$R = 0, 1, 2 \ldots$ – neighbourhood radius,

$d(c, m)$ is the distance between winning neuron c and neuron m in the Kohonen map.

η-learning coefficient in the range $(0-1)$

G – neighbourhood gaussian function,

x – input vector,

w-weight vector.

A schematic of the proposed SOM-based fault-classification system is shown in Fig. 15. It should be emphasized that during the training process of the network, only the symptoms derived from the mathematical modeling of the PMSM were used, whereas the verification data were obtained during the measurements of the real object for different values of the load torque and rotational speed.
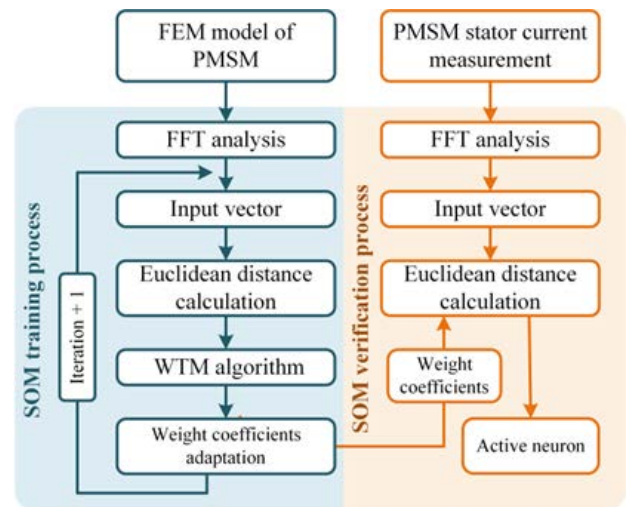

FIGURE 15. Schematic of SOM-based PMSM fault diagnostic system trained with simulation patterns and tested with experimental patterns.

After the training process, the vector of the obtained SOM weighting factor is used in the verification process. In this case, only symptoms derived from measurements of the real object were used. Consequently, it is possible to accurately determine the suitability of the Kohonen network structure designed based on the simulation patterns in the real drive-fault classification process in terms of future practical implementation.

B. THE EXPERIMENTAL VERYFICATION OF THE SOM-BASED DIAGNOSTIC SYSTEM

The development of a classification system based on the self-organizing Kohonen network involves determining the characteristic zones of the map that are related to the class under consideration. This process is not automatic and forces

the empirical elaboration of the zones of Kohonen's map. In the application presented herein, the average value of the Euclidean distance measures between the samples of the training set based on the field-circuit model and network neurons was used to develop the Kohonen map areas. The Euclidean distance matrix obtained for each damage category was normalized using the hyperbolic tangent function. After normalization, the zone characteristics of the Kohonen map for the individual damage categories were plotted automatically, as shown in Fig. 16.
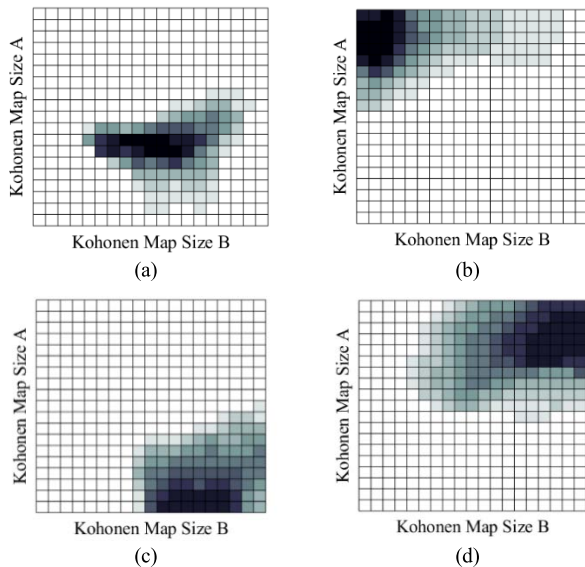
FIGURE 16. SOM area characteristics of the considered PMSM damage categories obtained during the training process with the simulation dataset: (a) unfaulty motor, (b) demagnetization, (c) stator winding fault, (d) mixed damages: T_L = var ($0-T_{LN}$ with a step of $0.1T_{LN}$), f_s = var ($50-100$ Hz with a step of 10 Hz).

FIGURE 17. Classification of PMSM fault based on SOM for testing (measurement-based) data: (a) demagnetization, (b) stator winding fault, (c) mixed damage: T_L = var ($0-T_{LN}$ with a step of $0.1T_{LN}$), f_s = var ($50-100$ Hz with a step of 10 Hz).

The dark zones of the map observed in Fig. 16 correspond to the smallest value of the Euclidean distance measure, that is, to the places where neurons belonging to the appropriate class are activated.

Experimental tests were performed for the results of measurements (testing data vector) on the real PMSM drive for variable load torque conditions and the frequency of the supply voltage, different from those used in the training process, according to the methodology presented in Fig. 15. The results of the damage classification using the developed SOM are shown in Fig. 17.

The analysis of SOM responses in the form of active neurons presented in Fig. 17 shows a clear separation of areas characteristic of individual categories. The map area assigned to the undamaged state (blue) is located at the center of the map and is the reference point for the remaining categories. As shown in Figs. 17a and 17c, owing to the increase in the degree of damage to the stator windings, neurons located further from the area characteristic of the unfaulty state (moving away from the zone marked in blue) were activated. This phenomenon is observed for both the training and testing data (Fig. 16c,d and Fig. 17b,c), and may indicate the possibility
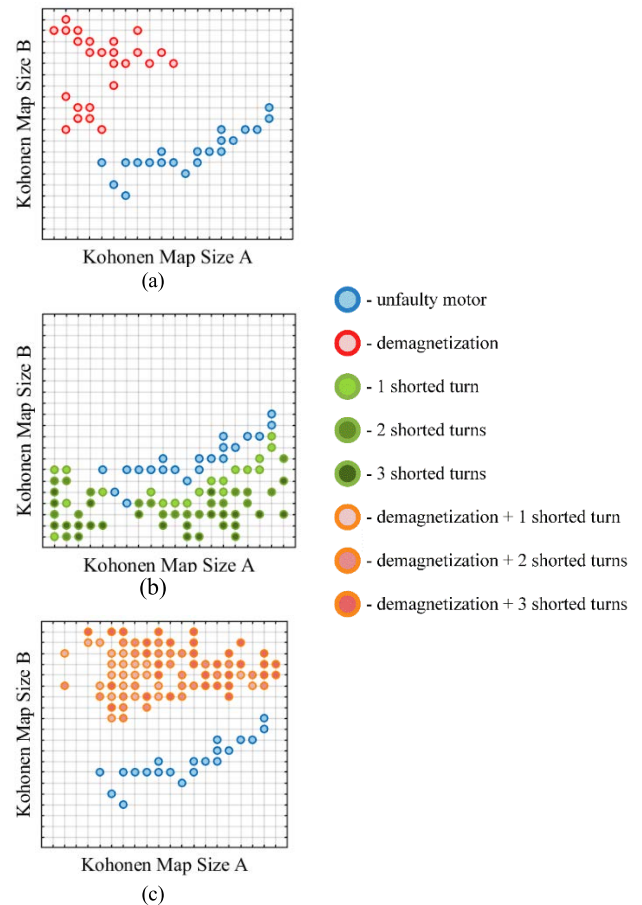
of both stator winding damage detection and an approximate assessment of the degree of damage. However, it should be noted that the effectiveness of assessing the degree of damage to the stator windings will strongly depend on the actual value of the load torque and the frequency of the supply voltage, which is particularly noticeable in the experimental tests conducted for a real motor or in the results of FEM-circuit modeling. This influence was also observed for the simplified circuit model in the case of the most sensitive fault amplitude of the $3f_s$ harmonics, as presented in [8].

PM damage is characterized by clear changes in the waveforms of the phase currents, and thus, significant changes in the values of the elements of the SOM input vector. Therefore, the separation of the area characteristic of demagnetization from the state of no damage was more significant (Fig. 17a). In addition, the areas characteristic of demagnetization and damage to the stator windings are located in the extreme parts of the map. This is undoubtedly advantageous in terms of recognizing the type of defect and limiting the risk of incorrect classifications.

Simultaneous damage to the rotor magnet and stator windings results in the activation of neurons in an area that does

not belong to any of the considered categories (Figs. 16d and 17c). As in the case of ITSCs (Figs. 16c and 17b), along with an increase in the number of shorted turns, distancing of the active neurons from the zone characteristic of demagnetization is observed. Therefore, it is possible to approximate the degree of stator damage even in the case of simultaneous PM failure.

The analysis of active neurons shows that an increase in the degree of the defect, regardless of the type of damage, results in moving away from the zone characteristic of an unfaulty state towards the outer boundaries of the Kohonen map. This trend was evident for both training and test samples. Moreover, as shown in Fig. 17, the Kohonen maps did not visually reflect the 288 test samples used during the experimental verification. This is related to the overlap of the active neurons of the Kohonen map in the case of a slight difference in the network input vector. Such a situation is observed inter alia in the case of similar operating conditions $f_s = 50 \text{ Hz } T_L = 0.8 \, T_{LN}$ and $f_s = 60 \text{ Hz}, T_L = 0.6 \, T_{LN}$, where the differences in the amplitudes constituting the elements of the input vector are almost identical. The phenomenon of Kohonen map overlapping neurons was discussed in detail in [16].

Furthermore, it should be highlighted that the experimental verification confirmed the high efficiency of PMSM damage classification by SOM based on training data from mathematical modeling, even for incipient faults, which is the original result presented in this article.

C. THE IDEA OF NEURAL CLASSIFIER BASED ON MULTILAYER PERCEPTRON

Multilayer perceptron (MLP) is one of the most widely used neural structures in the diagnostics of electrical machines. This is because of its popularity as a simple mathematical description, easy practical implementation, and the ability to approximate any function. However, ensuring the high precision of MLP-based diagnostic systems requires the development of input vectors, whose elements can be assigned to one of the considered groups. The current approach to the implementation of MLP in diagnostics is based on the use of data from the same test object in the form of a real or mathematical model in both training and testing processes. The use of data from mathematical modeling in the training process and verification in a real motor drive results in many difficulties owing to the measurement noise and inaccuracy of the mathematical models [14]. However, only this approach makes sense for practical implementation of neural structures, as explained in the Introduction. It should be noted that the presence of measurement disturbances and small errors in the data acquisition should not significantly affect the operation of the system. Therefore, it is important to develop an NN structure in which there is a trade-off between precision and generalization. To show the approximation ability of the MLP acquired in the training process based on a simulation dataset for unknown data from a real object, the research was conducted according to the idea presented in Fig. 18.
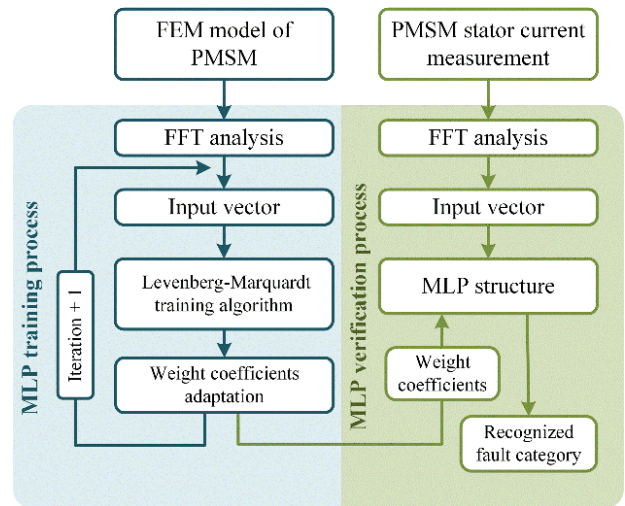

FIGURE 18. Schematic of MLP-based PMSM fault diagnosis system trained using simulation patterns and tested with experimental patterns.

The training and verification processes of the MLP-based PMSM damage classifier were divided into two stages in a manner similar to that presented for the SOM. In the training process, data from the PMSM modeling were used. The input vector of the network contained the amplitudes of the phase-current spectrum at the frequencies f_r, f_s, $3f_s + 2f_r$, and $3f_s$. The input vectors of the network were selected based on many simulation studies for various operating conditions of the PMSM ($T_L = (0–1)T_{LN}$ with $0.2T_{LN}$ step, $f_s = (0.5–1)f_{sN}$ with $0.1f_{sN}$ step). It should be emphasized that extracting symptoms from a diagnostic signal requires precise knowledge of the nature of the damage and its influence on the diagnostic signal. In the absence of visible changes in the signal, the development of a neural structure is extremely difficult in practical applications. The course of the MLP learning process takes place through the presentation of the NN of all input vectors and the corresponding system reactions. The parameters of the multilayer perceptron and the training process are listed in Table 2.

TABLE 2. Parameters of multilayer perceptron.

Name of parameter	Value
Structure (number of neurons in layers)	{4}-{4}-{6}-{1}
Input vector size	1×4
Input vector normalization	[-1,1]
Activation function	Hyperbolic tangent
Training algorithm	Levenberg-Marquardt
Number of training epochs	700
Training data (simulation) packet size	288
Testing data (real measurements) packet size	288
Number of considered fault categories	4

In the course of simulation studies carried out for more than 200 different neural structures, an MLP network containing two hidden layers with four and six neurons and an activation function in the form of a hyperbolic tangent

was selected. The output layer of the network contained one neuron whose activation state corresponded to each of the four damage categories considered. During the training process, the weighting factors of all the layers were subjected to adaptation according to a specific algorithm. The use of a differentiable activation function, the Levenberg-Marquardt algorithm was used for 700 training epochs, owing to the use of a differentiable activation function. After the training process, the structure of the network with appropriately selected weighting factors constitutes a part of the neural fault classifier that works with the measurement data from the real object.

D. THE EXPERIMENTAL VERYFICATION OF THE MLP-BASED DIAGNOSTIC SYSTEM

The effectiveness of the MLP-based diagnostic system was verified during laboratory tests on a stand with a PMSM operating under various load and rotational speed conditions, which were different from those under the training process. The tests were divided into eight stages, depending on the type of physically modeled PMSM damage: unfaulty motor ($N_{sh} = 0$, $N_{dem} = 0$), incipient ITSC ($N_{sh} = 1,2,3$, $N_{dem} = 0$), demagnetization ($N_{sh} = 0$, $N_{dem} = 1$), and mixed damage ($N_{sh} = 1,2,3$, $N_{dem} = 1$). Each stage contained 36 samples for different machine operating conditions in the stator frequency and load torque ranges of $f_s = (50–100)$ Hz (with steps of 10 Hz) and $T_L = (0–1)T_{LN}$ (with steps of $0.2T_{LN}$). The effectiveness of the diagnostic system was evaluated in two categories: damage-detection precision, which is the ability to recognize the failure state and its absence, and classification precision, which is the ability to determine the type of failure. A summary of the neural network responses to data obtained from a real object is shown in Fig. 19.
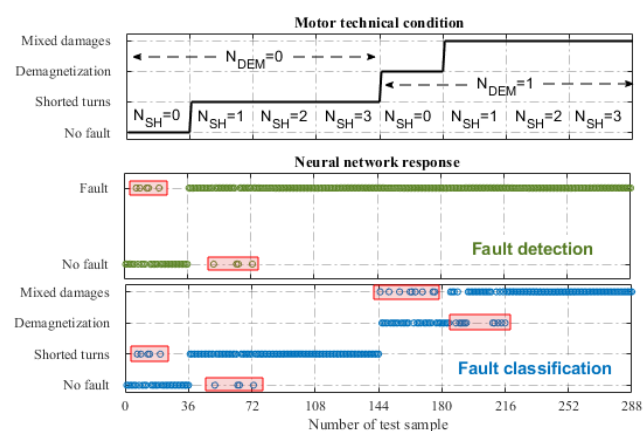

FIGURE 19. Experimental verification of the MLP-based PMSM fault diagnostic system: T_L = var (0−T_{LN} with steps of 0.1T_{LN}), f_s = var (50− 100 Hz with steps of 10 Hz).

An analysis of the results of the experimental studies presented in Fig. 19 confirmed the correctness of the proposed diagnostic approach. The detection efficiency of the MLP-based system was determined to be 96.9%. The neural network correctly classified the type of damage in more than 88.6% of cases. As shown in Fig. 19, the misinformation regarding the PMSM condition consisted mainly of distinguishing between one shorted turn ($N_{sh} = 1$) and no damage to the stator windings ($N_{sh} = 0$). This phenomenon was observed in cases of single and mixed damage. However, it should be noted that the state of one shorted turn is particularly difficult to recognize because of slight changes in the diagnostic signal (stator current) compared to the healthy state of the motor.

In addition, demagnetization has a much greater impact on the elements of the input vector, which makes it difficult to recognize the initial degree of ITSCs when the magnet is damaged. An in-depth analysis of the test results allowed us to observe the lack of influence of machine operating conditions on the accuracy of the diagnostic system, which is a significant advantage of the proposed approach. Despite the occurrence of single classification errors, the proposed structure is characterized by excellent classification and generalization capabilities.

The possibility of performing the training process on the mathematical model while simultaneously maintaining high precision for a real object is an unquestionable advantage of the proposed approach concerning diagnostic applications described in the literature. However, it should be noted that the FEM model requires a long computational time, which significantly extends the time required to implement diagnostic applications. Moreover, the extraction of fault symptoms based on spectral analysis can only be used in steady-state machine operating conditions. It is possible to omit this limitation by using high-order signal analysis methods, such as the Hilbert-Huang transform or wavelet transform [3].

The fault detection system presented in this article is based on a multilayer perceptron that ensures full automation of the diagnostic process. In the case of self-organizing maps, the system response is difficult to analyze because of the type of NN output information (active neurons on Kohonen maps). In future work, the authors will propose the cascade-connected NN structure based on SOM and MLP to fully automate the developed diagnostic system (trained with simulation data – transferred to real object data), similarly as it was done in for classical approach (trained and tested with real object data) [33].

V. CONCLUSION

This article presents the practical application of a shallow NN-based fault detector and classifier trained with sample patterns obtained by FEM-circuit simulation in the PMSM fault detection process. The use of information from mathematical models is advantageous in terms of generating diagnostic patterns for any machine operating condition. The possibilities offered by the FEM-circuit calculations can also be used to map the physical phenomena occurring at the time of motor defects. In addition, the use of mathematical models allows for obtaining symptoms and abandoning the

physical modeling of damages to the analyzed object, which, especially in the case of higher-power motors, could be expensive and dangerous.

The results of the simulation tests obtained based on the FEM-circuit model corresponded to the situation in which the drive operated under ideal conditions. These models ignore the influence of measurement disturbances, sensor errors, and the electrical and mechanical asymmetry of the machines. The influence of external conditions is visible in the FFT spectra of the measured stator current in the form of an increased level of measurement noise (Section II). However, they did not influence the quality of the damage symptoms. Including these phenomena in the mathematical model is possible, but the time required for the FEM calculations would be much longer.

The application of the SOM Kohonen network taught based on the results of the simulation studies presented in this article was characterized by the very high efficiency of the PMSM damage classification. In addition, SOM analysis provides automation of the motor technical condition assessment process, characterized by a very simple mathematical description and a small amount of training data that ensures very high classification precision. The possibility of using Euclidean distance to develop the areas of Kohonen map characteristics for the considered fault categories allows one to fully automate the diagnostic process and accelerate the NN implementation process.

The diagnostic application based on MLP is characterized by the simplicity of its implementation in programmable systems, as well as the mapping capabilities of any function. The MLP network approximates the learning data and the learning process involves minimizing a suitable cost function. In connection with the idea of the MLP operation, the NN structure requires well-chosen signals in terms of changes owing to damage (preferably linear changes). During the experimental tests, the MLP-based diagnostic system was characterized by a correct assessment of the degree of failure in more than 88.6% of the cases, whereas the fault detection accuracy exceeded 96.9%. It should be emphasized that the experimental verification of the MLP and SOM structures was performed under various PMSM operating conditions in contrast to the simulation-based training process.

The results of the experimental research presented in this article confirm the possibility of practical implementation of the proposed diagnostic methodology for PMSM drives. Furthermore, the possibility of using the field-circuit model as a source of diagnostic patterns applied during the NN training process constitutes a definitive advantage of the proposed method.

The proposed NN-based fault detection system was implemented with the cooperation of VeriStand and MATLAB programming environments. Nevertheless, future research will focus on the implementation of the measurement and diagnostic system in the form of a separate device based on the generally available (low-cost) industrial processor advanced RISC machines (ARM).

APPENDIX

TABLE 3. Parameters of PMSM motors lenze 14H15.

Name of parameter	Symbol	Value	Units
Power	P_N	2500	W
Torque	T_N	16	Nm
Speed	n_N	1500	r/min
Stator phase voltage	U_{sN}	325	V
Stator current	I_{sN}	6.6	A
Frequency	f_{sN}	100	Hz
Pole pairs number	p_p	4	–
Number of stator winding turns	N_s	2x125	–
Inertia	J	1.42	kg cm^2
Remanent magnetization	B_r	1,27	T
Stator resistance	R_s	1.206	Ω
Stator inductance	L_s	7.02	mH

REFERENCES

[1] W. T. Thomson and I. Culbert, *Current Signature Analysis for Condition Monitoring of Cage Induction Motors: Industrial Application and Case Histories*. Hoboken, NJ, USA: Wiley, 2017.

[2] R. Isermann, *Fault-Diagnosis Applications: Model-Based Condition Monitoring: Actuators, Drives, Machinery, Plants, Sensors, and Fault-Tolerant Systems*. Berlin, Germany: Springer, 2011.

[3] T. Orlowska-Kowalska, M. Wolkiewicz, P. Pietrzak, M. Skowron, P. Ewert, G. Tarchala, M. Krzysztofiak, and C. T. Kowalski, "Fault diagnosis and fault-tolerant control of PMSM drives–state of the art and future challenges," *IEEE Access*, vol. 10, pp. 59979–60024, 2022.

[4] A. Usman, B. M. Joshi, and B. S. Rajpurohit, "Review of fault modeling methods for permanent magnet synchronous motors and their comparison," in *Proc. IEEE 11th Int. Symp. Diag. for Electr. Mach., Power Electron. Drives (SDEMPED)*, Aug. 2017, pp. 141–146.

[5] J. Hang, J. Zhang, M. Cheng, and J. Huang, "Online interturn fault diagnosis of permanent magnet synchronous machine using zero-sequence components," *IEEE Trans. Power Electron.*, vol. 30, no. 12, pp. 6731–6741, Dec. 2015.

[6] L. Romeral, J. C. Urresty, J.-R. R. Ruiz, and A. G. Espinosa, "Modeling of surface-mounted permanent magnet synchronous motors with stator winding interturn faults," *IEEE Trans. Ind. Electron.*, vol. 58, no. 5, pp. 1576–1585, May 2011.

[7] W. Liu, L. Liu, I.-Y. Chung, D. A. Cartes, and W. Zhang, "Modeling and detecting the stator winding fault of permanent magnet synchronous motors," *Simul. Model. Pract. Theory*, vol. 27, pp. 1–16, Sep. 2012.

[8] M. Krzysztofiak, M. Skowron, and T. Orlowska-Kowalska, "Analysis of the impact of stator inter-turn short circuits on PMSM drive with scalar and vector control," *Energies*, vol. 14, no. 1, pp. 1–20, Jan. 2021.

[9] K.-C. Kim, S.-B. Lim, D.-H. Koo, and J. Lee, "The shape design of permanent magnet for permanent magnet synchronous motor considering partial demagnetization," *IEEE Trans. Magn.*, vol. 42, no. 10, pp. 3485–3487, Oct. 2006.

[10] J.-H. Yoo and T.-U. Jung, "Demagnetization diagnosis of permanent magnet synchronous motor using frequency analysis at standstill condition," *J. Magn.*, vol. 21, no. 2, pp. 249–254, Jun. 2016.

[11] S. S. Moosavi, A. Djerdir, Y. A. Amirat, and D. A. Khaburi, "Demagnetization fault investigation in permanent magnet synchronous motor," in *Proc. 5th Annu. Int. Power Electron., Drive Syst. Technol. Conf. (PEDSTC)*, Feb. 2014, pp. 617–623.

[12] J. A. Rosero, L. Romeral, J. A. Ortega, and E. Rosero, "Short-circuit detection by means of empirical mode decomposition and Wigner–Ville distribution for PMSM running under dynamic condition," *IEEE Trans. Ind. Electron.*, vol. 56, no. 11, pp. 4534–4547, Nov. 2009.

[13] Y.-S. Lee, K.-T. Kim, and J. Hur, "Finite-element analysis of the demagnetization of IPM-type BLDC motor with stator turn fault," *IEEE Trans. Magn.*, vol. 50, no. 2, pp. 889–892, Feb. 2014.

[14] S. S. Moosavi, A. Djerdir, Y. Ait-Amirat, and D. Khaburi, "ANN based fault diagnosis of permanent magnet synchronous motor under stator winding shorted turn," *Electr. Power Syst. Res.*, vol. 125, pp. 67–82, Aug. 2015.

[15] M. Skowron, M. Wolkiewicz, T. Orlowska-Kowalska, and C. T. Kowalski, "Effectiveness of selected neural network structures based on axial flux analysis in stator and rotor winding incipient fault detection of inverter-fed induction motors," *Energies*, vol. 12, no. 12, p. 2392, Jun. 2019.

[16] M. Skowron, M. Wolkiewicz, T. Orlowska-Kowalska, and C. Kowalski, "Application of self-organizing neural networks to electrical fault classification in induction motors," *Appl. Sci.*, vol. 9, no. 4, p. 616, Feb. 2019.

[17] O. Sid, M. Menaa, S. Hamdani, O. Touhami, and R. Ibtiouen, "Self-organizing map approach for classification of electricals rotor faults in induction motors," in *Proc. 2nd Int. Conf. Electric Power Energy Convers. Syst. (EPECS)*, Nov. 2011, pp. 1–6.

[18] S. Wu and T. W. S. Chow, "Induction machine fault detection using SOM-based RBF neural networks," *IEEE Trans. Ind. Electron.*, vol. 51, no. 1, pp. 183–194, Feb. 2004.

[19] I.-H. Kao, W.-J. Wang, Y.-H. Lai, and J.-W. Perng, "Analysis of permanent magnet synchronous motor fault diagnosis based on learning," *IEEE Trans. Instrum. Meas.*, vol. 68, no. 2, pp. 310–324, Feb. 2019.

[20] B. A. Sa, C. M. V. Barros, C. A. Siebra, and L. S. Barros, "A multilayer perceptron-based approach for stator fault detection in permanent magnet wind generators," in *Proc. IEEE PES Innov. Smart Grid Technol. Conf.-Latin Amer. (ISGT Latin America)*, Sep. 2019, pp. 1–6.

[21] T. Shen, A. Kilic, C. Thulfaut, and H.-C. Reuss, "An intelligent diagnostic method for permanent magnet synchronous motors (PMSM) in the electric drive of autonomous vehicles," in *Proc. 21st Eur. Conf. Power Electron. Appl. (EPE ECCE Europe)*, Sep. 2019, pp. 1–10.

[22] C. Chuang, Z. Wei, W. Zhifu, and L. Zhi, "The diagnosis method of stator winding faults in PMSMs based on SOM neural networks," *Energy Proc.*, vol. 105, pp. 2295–2301, May 2017.

[23] J. Quiroga, D. A. Cartes, C. S. Edrington, and L. Liu, "Neural network based fault detection of PMSM stator winding short under load fluctuation," in *Proc. 13th Int. Power Electron. Motion Control Conf.*, Budapest, Hungary, Sep. 2008, pp. 793–798.

[24] Y. Nyanteh, C. Edrington, S. Srivastava, and D. Cartes, "Application of artificial intelligence to real-time fault detection in permanent-magnet synchronous machines," *IEEE Trans. Ind. Appl.*, vol. 49, no. 3, pp. 1205–1214, May 2013.

[25] S. S. Moosavi, A. Djerdir, Y. Aït-Amirat, and D. A. Kkuburi, "Artificial neural networks based fault detection in 3-phase PMSM traction motor," in *Proc. 20th Int. Conf. Electr. Mach. (ICEM)*, Sep. 2012, pp. 1579–1585.

[26] M. Akar, M. Hekim, and U. Orhan, "Mechanical fault detection in permanent magnet synchronous motors using equal width discretization-based probability distribution and a neural network model," *Turkish J. Electr. Eng. Comput. Sci.*, vol. 23, no. 3, pp. 813–823, 2015.

[27] M. Zhu, W. Hu, and N. C. Kar, "Acoustic noise-based uniform permanent-magnet demagnetization detection in SPMSM for high-performance PMSM drive," *IEEE Trans. Transport. Electrific.*, vol. 4, no. 1, pp. 303–313, Mar. 2018.

[28] T. K. Mersha and C. Du, "Co-simulation and modeling of PMSM based on Ansys software and simulink for EVs," *World Electric Vehicle J.*, vol. 13, no. 1, p. 4, Dec. 2021.

[29] P. Pietrzak and M. Wolkiewicz, "Comparison of selected methods for the stator winding condition monitoring of a PMSM using the stator phase currents," *Energies*, vol. 14, no. 6, p. 1630, 2021.

[30] X. Dai, Y. Zhang, L. Qiao, and D. Sun, "Fault diagnosis of permanent magnet synchronous motor based on improved probabilistic neural network," in *Proc. 40th Chin. Control Conf. (CCC)*, Jul. 2021, pp. 2767–2772.

[31] S. S. Refaat, H. Abu-Rub, M. S. Saad, E. M. Aboul-Zahab, and A. Iqbal, "Detection and discrimination between unbalanced supply and phase loss in PMSM using ANN-based protection scheme," in *Proc. 7th IEEE Conf. Exhib. (GCC)*, Nov. 2013, pp. 430–435.

[32] Z. Wang, J. Yang, C. Cao, and Z. Gu, "Phase-phase short fault analysis of permanent magnet synchronous motor in electric vehicles," *Energy Proc.*, vol. 88, pp. 915–920, Jun. 2016.

[33] M. Skowron and T. Orłowska-Kowalska, "Efficiency of cascaded neural networks in detecting initial damage to induction motor electric windings," *Electronics*, vol. 9, no. 8, p. 1314, Aug. 2020.

[34] P. Pietrzak, M. Wolkiewicz, and T. Orlowska-Kowalska, "PMSM stator winding fault detection and classification based on bispectrum analysis and convolutional neural network," *IEEE Trans. Ind. Electron.*, early access, Jul. 13, 2022, doi: 10.1109/TIE.2022.3189076.

MACIEJ SKOWRON received the M.Sc. and Ph.D. degrees from the Faculty of Electrical Engineering, Wroclaw University of Science and Technology, Poland, in 2018 and 2021, respectively. Since 2021, he has been an Assistant Professor with the Department of Electrical Machines, Drives, and Measurements. His research interests include diagnostics of AC motor drives, signal processing methods, artificial intelligence, digital implementation of control, and diagnostic systems.

MATEUSZ KRZYSZTOFIAK received the M.Sc. degree in automation and robotics from the Wroclaw University of Science and Technology, in 2019, where he is currently pursuing the Ph.D. degree with the Department of Electrical Machines, Drives and Measurements. His research interests include monitoring and fault diagnosis of electrical machines, in particular PMSM analysis based on mathematical models and the possibility to detect faults in a closed control structure.

TERESA ORLOWSKA-KOWALSKA (Life Senior Member, IEEE) received the Ph.D. and D.Sc. degrees in electrical engineering from the Wroclaw University of Technology (WUT), Wroclaw, Poland, in 1976 and 1990, respectively. Since 1993, she has been a Professor of electrical engineering and a Full Professor with WUT, since 2004, where she is the Head of the Electrical Drives Control Chair with the Faculty of Electrical Engineering. From 2002 to 2019, she was the Director of the Institute of Electrical Machines, Drives, and Measurements, WUT. She is the author of over 400 journal articles and conference proceedings, two textbooks, two books, and 50 chapters in monographs. Her research interests include controlled electrical drives, applications of the observer theory and artificial intelligence methods in sensorless control of AC drives, control methods of the drive systems with elastic couplings, diagnostics, and fault-tolerant control methods for AC drives. She has been a member of the Electrical Engineering Committee of the Polish Academy of Science, since 1996, the Council of Provosts of IV Division of the Polish Academy of Science, from 2011 to 2018, and the International Steering Committees of a few well-known conferences. From 2004 to 2014, she was an Associate Editor of the IEEE Transactions Industrial Electronics. She is a member of Editorial Boards of a few international journals and the Editor-in-Chief of *Power Electronics and Drives* journal. She serves as a reviewer of many IEEE, IET, Elsevier, Springer, Taylor & Francis, MDPI, SAGE, and other journals.

● ● ●